Dielectric screening in a layered lattice electron gas

2009 J. Phys.: Condens. Matter 21 385702

(http://iopscience.iop.org/0953-8984/21/38/385702)

J. Phys.: Condens. Matter **21** (2009) 385702 (7pp) doi:10.1088/0953-8984/21/38/385702

Dielectric screening in a layered lattice electron gas

Yi Gao[1] **and Wu-Pei Su**

Department of Physics and Texas Center for Superconductivity, University of Houston, Houston, TX 77204, USA

E-mail: flygaoonly@gmail.com

Received 22 June 2009
Published 24 August 2009
Online at stacks.iop.org/JPhysCM/21/385702

Abstract

We study the dielectric screening of an external point charge by a layered lattice electron gas in the random phase approximation. The screened potential at the neighboring sites of the point charge is found to be attractive under certain circumstances. We also investigate the impact of band structure on the screened potential. Our results provide a possible source of intersite attractive interactions in the extended Hubbard model.

(Some figures in this article are in colour only in the electronic version)

1. Introduction

The discovery of high-temperature superconductivity in cuprates [1] and the rapid raising of the transition temperature to well above the melting point of nitrogen [2] ushered in an era of great excitement for the condensed-matter physics community. During the following years, there has been a frenetic race in the preparation and synthesis of compounds with increasingly higher critical temperatures. While there are hundreds of high-T_c compounds, they all share a layered structure made up of one or more copper–oxygen planes. Recently, high-temperature superconductivity has been reported in a family of Fe-based oxypnictides [3–8] which also consist of layered quasi-two-dimensional FeAs or FeP planes. All these suggest the layered two-dimensional structure may play an important role in understanding high-temperature superconductivity. Also, single-layer graphene and bilayer graphene have attracted a great deal of attention, both experimentally and theoretically, for technological applications and fundamental interest [9–17].

Until now, most theoretical studies of the high-temperature superconductivity in cuprates start from the Hubbard model. And the extended Hubbard model, which is the regular Hubbard model supplemented with an intersite attractive interaction, has been applied to account for both antiferromagnetic and d-wave superconducting states [18–20]. The origin of the intersite attractive interaction, previously, is thought to be caused by electron–lattice coupling. Such coupling results in short-ranged attractive interaction between electrons, when competing with the repulsive Coulomb interaction, can lead to an overall short-ranged attractive interaction [21–27].

Here, we propose another possible source of the intersite attractive interaction, which arises from a purely electronic mechanism, that is, dielectric screening of the electron–electron interaction. In contrast to the previous work dealing with dielectric screening of the Coulomb interaction in a two-dimensional electron gas with an energy dispersion $E(\boldsymbol{k}) \sim k^2$ [28–30], or in graphite intercalation compounds which have $E(\boldsymbol{k}) \sim k$ [31], we investigate the dielectric screening of a Yukawa potential in a layered lattice electron gas by using a tight-binding model in the random phase approximation. It has been known for some time in both the cuprates and the oxypnictides that a tight-binding approach with electron–electron interaction added is a more appropriate picture than that of nearly-free-electron metals [18, 32, 33].

2. Methodology

We consider electrons moving in layers of a two-dimensional square lattice, with lattice constant a and interlayer distance r_0. Each of those planes has N lattice sites along both the $\boldsymbol{e}_x$ and $\boldsymbol{e}_y$ directions. Without loss of generality, we suppose N being odd. Besides, we use integer m to label the planes, $m = 0, \pm1, \pm2, \ldots$. The in-plane lattice site vector is $\boldsymbol{R}_i = i_x a\boldsymbol{e}_x + i_y a\boldsymbol{e}_y$, where i_x and i_y are both integers and $i_x, i_y = -(N-1)/2, \ldots, 0, \ldots, (N-1)/2$. We set the origin to be

[1] Author to whom any correspondence should be addressed.

at the center of the $m = 0$ plane, at the $(i_x, i_y) = (0, 0)$ lattice site. The electrons are allowed to move in each of the planes, but cannot hop between them. The tight-binding Hamiltonian can then be written as

$$\hat{H}_0 = -t \sum_m \sum_\sigma \sum_i \sum_\delta \hat{c}^\dagger_{mi\sigma} \hat{c}_{mi+\delta\sigma}, \tag{1}$$

where t is the nearest-neighbor hopping integral, the integer m labels the planes, $\hat{c}^\dagger_{mi\sigma}$ creates an electron with spin σ at lattice site $\boldsymbol{R}_i$ of the mth plane and δ represents a two-dimensional nearest-neighbor vector. $\hat{H}_0$ is diagonal in the momentum space:

$$\hat{H}_0 = \sum_m \sum_\sigma \sum_{\boldsymbol{k}\in \mathrm{BZ}} E(\boldsymbol{k}) \hat{c}^\dagger_{m\boldsymbol{k}\sigma} \hat{c}_{m\boldsymbol{k}\sigma}, \tag{2}$$

where BZ stands for the first Brillouin zone, $\boldsymbol{k}$ is a two-dimensional in-plane wavevector, $-\pi < \boldsymbol{k} \cdot a\boldsymbol{e}_i \leqslant \pi$ (with $i = x, y$) and

$$E(\boldsymbol{k}) = -t \sum_\delta \mathrm{e}^{-\mathrm{i}\boldsymbol{k}\cdot\delta} = -2t(\cos k_x a + \cos k_y a). \tag{3}$$

The eigenvectors of $\hat{H}_0$ can be represented as $|m, \boldsymbol{k}_n, \sigma\rangle$ with $\boldsymbol{k}_n \in$ BZ and $n = 1, 2, \ldots, N^2$. With that, the one-particle density matrix [28] can be represented as

$$\hat{\rho}_0 = \sum_m \sum_\sigma \sum_{\boldsymbol{k}\in \mathrm{BZ}} f_{\boldsymbol{k}} |m\boldsymbol{k}\sigma\rangle\langle m\boldsymbol{k}\sigma|, \tag{4}$$

where $f_{\boldsymbol{k}} = \{\exp[(E(\boldsymbol{k}) - E_\mathrm{f})/(K_B T)] + 1\}^{-1}$ is the Fermi distribution function, E_f is the Fermi energy and T is temperature.

We now introduce an external point charge (impurity) into the system. For simplicity, we suppose it is located at the origin with a negative unit charge $-e$. The bare potential seen by another negative unit point charge at $\boldsymbol{R}_i$ of the mth plane is

$$V^{\mathrm{ext}}_m(\boldsymbol{R}_i) = \frac{e^2 \exp(-\lambda|\boldsymbol{R}_i + mr_0\boldsymbol{e}_z|)}{|\boldsymbol{R}_i + mr_0\boldsymbol{e}_z|}, \tag{5}$$

where e is the unit charge and $\boldsymbol{e}_z$ is the unit vector perpendicular to the planes. To speed up the convergence of the series, we suppose the interaction between all charges takes a Yukawa form. As we are only interested in the potential near the impurity, the Yukawa form should not make a significant difference for $\lambda = 0.2a^{-1}$.

The perturbation of the impurity causes a change in the charge density in each plane, which in turn induces a new potential at $\boldsymbol{R}_i$ of the mth plane:

$$V^{\mathrm{ind}}_m(\boldsymbol{R}_i) = \sum_p \sum_j \frac{e^2 \Delta N_p(\boldsymbol{R}_j) \exp(-\lambda|\boldsymbol{R}_j - \boldsymbol{R}_i + (p-m)r_0\boldsymbol{e}_z|)}{|\boldsymbol{R}_j - \boldsymbol{R}_i + (p-m)r_0\boldsymbol{e}_z|}, \tag{6}$$

where $\Delta N_p(\boldsymbol{R}_j)$ is the charge density change at $\boldsymbol{R}_j$ in the pth plane. The total potential is

$$V^{\mathrm{tot}}_m(\boldsymbol{R}_i) = V^{\mathrm{ext}}_m(\boldsymbol{R}_i) + V^{\mathrm{ind}}_m(\boldsymbol{R}_i). \tag{7}$$

The total Hamiltonian is now

$$\hat{H} = \hat{H}_0 + \hat{H}', \tag{8}$$

$$\hat{H}' = \hat{H}^{\mathrm{ext}} + \hat{H}^{\mathrm{ind}}, \tag{9}$$

where

$$\hat{H}^{\mathrm{ext}} = \sum_m \sum_i \sum_\sigma V^{\mathrm{ext}}_m(\boldsymbol{R}_i) \hat{c}^\dagger_{mi\sigma} \hat{c}_{mi\sigma}, \tag{10}$$

and

$$\hat{H}^{\mathrm{ind}} = \sum_m \sum_i \sum_\sigma V^{\mathrm{ind}}_m(\boldsymbol{R}_i) \hat{c}^\dagger_{mi\sigma} \hat{c}_{mi\sigma}. \tag{11}$$

$\hat{H}'$ causes a perturbation $\hat{\rho}'$ to the density matrix $\hat{\rho}_0$. According to the equation of motion for $\hat{\rho} = \hat{\rho}_0 + \hat{\rho}'$, to first order, we have

$$[\hat{H}_0, \hat{\rho}'] = [\hat{\rho}_0, \hat{H}'], \tag{12}$$

or, equivalently, in the eigenspace of $\hat{H}_0$, it can be expressed as

$$\begin{aligned}
&\langle m_1, \boldsymbol{k}_1, \sigma_1|\hat{H}_0\hat{\rho}' - \hat{\rho}'\hat{H}_0|m_2, \boldsymbol{k}_2, \sigma_2\rangle \\
&\quad = \langle m_1, \boldsymbol{k}_1, \sigma_1|\hat{\rho}_0\hat{H}' - \hat{H}'\hat{\rho}_0|m_2, \boldsymbol{k}_2, \sigma_2\rangle, \\
&(E(\boldsymbol{k}_1) - E(\boldsymbol{k}_2))\hat{\rho}'_{m_1\boldsymbol{k}_1\sigma_1, m_2\boldsymbol{k}_2\sigma_2} \\
&\quad = (f_{\boldsymbol{k}_1} - f_{\boldsymbol{k}_2})\hat{H}'_{m_1\boldsymbol{k}_1\sigma_1, m_2\boldsymbol{k}_2\sigma_2}, \\
&\hat{H}^{\mathrm{ext}}_{m_1\boldsymbol{k}_1\sigma_1, m_2\boldsymbol{k}_2\sigma_2} = \delta_{m_1m_2}\delta_{\sigma_1\sigma_2}\frac{1}{N^2} \\
&\qquad \times \sum_i V^{\mathrm{ext}}_{m_1}(\boldsymbol{R}_i)\mathrm{e}^{-\mathrm{i}(\boldsymbol{k}_2-\boldsymbol{k}_1)\cdot\boldsymbol{R}_i} = V^{\mathrm{ext}}_{m_1\boldsymbol{q}}, \\
&\hat{H}^{\mathrm{ind}}_{m_1\boldsymbol{k}_1\sigma_1, m_2\boldsymbol{k}_2\sigma_2} = \delta_{m_1m_2}\delta_{\sigma_1\sigma_2}\frac{1}{N^2} \\
&\qquad \times \sum_i V^{\mathrm{ind}}_{m_1}(\boldsymbol{R}_i)\mathrm{e}^{-\mathrm{i}(\boldsymbol{k}_2-\boldsymbol{k}_1)\cdot\boldsymbol{R}_i} = V^{\mathrm{ind}}_{m_1\boldsymbol{q}},
\end{aligned} \tag{13}$$

$\boldsymbol{q} = \boldsymbol{k}_2 - \boldsymbol{k}_1$

and

$$\begin{aligned}
\Delta N_p(\boldsymbol{R}_j) &= \mathrm{Tr}[\hat{\rho}' \sum_\sigma \hat{c}^\dagger_{pj\sigma}\hat{c}_{pj\sigma}] \\
&= \frac{1}{N^2} \sum_{\boldsymbol{k}_3, \boldsymbol{k}_4\in \mathrm{BZ}} \sum_\sigma \hat{\rho}'_{p\boldsymbol{k}_3\sigma, p\boldsymbol{k}_4\sigma} \mathrm{e}^{\mathrm{i}(\boldsymbol{k}_4-\boldsymbol{k}_3)\cdot\boldsymbol{R}_j} \\
&= \frac{1}{N^2} \sum_{\boldsymbol{k}_3, \boldsymbol{k}_4\in \mathrm{BZ}} \sum_\sigma \frac{f_{\boldsymbol{k}_3} - f_{\boldsymbol{k}_4}}{E(\boldsymbol{k}_3) - E(\boldsymbol{k}_4)} \hat{H}'_{p\boldsymbol{k}_3\sigma, p\boldsymbol{k}_4\sigma} \mathrm{e}^{\mathrm{i}(\boldsymbol{k}_4-\boldsymbol{k}_3)\cdot\boldsymbol{R}_j}.
\end{aligned} \tag{14}$$

Following the standard treatment of random phase approximation as described in [28, 34], inserting (14) into (6), together with (13), we derive the following self-consistent equations:

$$V^{\mathrm{tot}}_{m\boldsymbol{q}} = F_m(\boldsymbol{q}) + D(\boldsymbol{q}) \sum_p F_{m-p}(\boldsymbol{q}) V^{\mathrm{tot}}_{p\boldsymbol{q}}, \tag{15}$$

where $V^{\mathrm{tot}}_{m\boldsymbol{q}}$ is the Fourier transformation of the total potential in the mth plane. $F_m(\boldsymbol{q})$ is the Fourier transformation of the Yukawa potential:

$$F_m(\boldsymbol{q}) = \frac{e^2}{N^2} \sum_i \frac{\exp(-\lambda|\boldsymbol{R}_i + mr_0\boldsymbol{e}_z|)}{|\boldsymbol{R}_i + mr_0\boldsymbol{e}_z|} \mathrm{e}^{-\mathrm{i}\boldsymbol{q}\cdot\boldsymbol{R}_i}, \tag{16}$$

and

$$D(\boldsymbol{q}) = 2 \sum_{\boldsymbol{k}\in \mathrm{BZ}} \frac{f_{\boldsymbol{k}} - f_{\boldsymbol{k}-\boldsymbol{q}}}{E(\boldsymbol{k}) - E(\boldsymbol{k}-\boldsymbol{q})}, \qquad \boldsymbol{q} \in \mathrm{BZ}. \tag{17}$$

After solving the equations for $V_{mq}^{\rm tot}$, we can obtain the total potential at $\boldsymbol{R}_i$ of the mth plane by Fourier-transforming back into the real space:

$$V_m^{\rm tot}(\boldsymbol{R}_i) = \sum_{q\in {\rm BZ}} V_{mq}^{\rm tot} {\rm e}^{{\rm i}q\cdot R_i}, \tag{18}$$

this total potential is actually the screened potential.

3. Results and discussion

Below we carry out numerical calculations and analyze the obtained results. The parameters used in our model are: in-plane lattice constant $a = 3.84$ Å and the nearest-neighbor hopping integral $t = 0.3$ eV; these are numbers typical for the cuprates. The Yukawa screening constant is set to be $\lambda = 0.2a^{-1}$. The number of lattice sites along the $\boldsymbol{e}_x$ ($\boldsymbol{e}_y$) direction is $N = 201$, and we adopt periodic conditions in the two-dimensional lattice. Due to the discreteness of the lattice, the calculation of the Fourier transform of the Yukawa potential $F_m(\boldsymbol{q})$ cannot be converted into an integral as in [28], the summation over lattice site i can only be done numerically:

$$F_m(\boldsymbol{q}) = \frac{e^2}{N^2 a}\sum_{i_x}\sum_{i_y}\frac{\exp(-\lambda a\sqrt{i_x^2+i_y^2+(m\frac{r_0}{a})^2})}{\sqrt{i_x^2+i_y^2+(m\frac{r_0}{a})^2}} \times {\rm e}^{-{\rm i}a\boldsymbol{q}\cdot(i_x\boldsymbol{e}_x+i_y\boldsymbol{e}_y)}. \tag{19}$$

When $m = 0$ and $i_x = i_y = 0$, this term in the summation is formally infinite. In the numerical calculations, we replace this term by a constant e^2U/a, corresponding to the on-site repulsive potential between two electrons. For $U = 2$, the on-site repulsive potential is about 7.5 eV.

First, we consider the one-layer case. In this case, the value of m can only be 0, so we have

$$V_{0q}^{\rm tot} = \frac{F_0(\boldsymbol{q})}{1 - D(\boldsymbol{q})F_0(\boldsymbol{q})}, \tag{20}$$

which is the standard two-dimensional dielectric screening in the random phase approximation. The difference between our model and the regular two-dimensional electron gas is that the wavevector $\boldsymbol{q}$ must be in the first Brillouin zone in our case while it can be arbitrary in the two-dimensional electron gas. Also when computing $D(\boldsymbol{q})$, we use the tight-binding dispersion instead of the free-electron dispersion in the denominator. The screened potential in the real space is then

$$V_0^{\rm tot}(\boldsymbol{R}_i) = \sum_{q\in {\rm BZ}} V_{0q}^{\rm tot} {\rm e}^{{\rm i}q\cdot R_i}. \tag{21}$$

In figure 1, we plot the screened potential energy at the six nearest-neighbors surrounding the impurity at the origin as a function of Fermi energy $E_{\rm f}$. Due to symmetry of the square lattice, we consider only the lattice sites between the two lines defined by $i_y = 0$ and $i_y = i_x$. First, because of the particle and hole symmetry, the potential energy is symmetric with respect to $E_{\rm f} = 0$. So, we can consider only negative $E_{\rm f}$. Second, there does exist an overscreening of the Yukawa potential, with a negative potential energy between two like external charges.

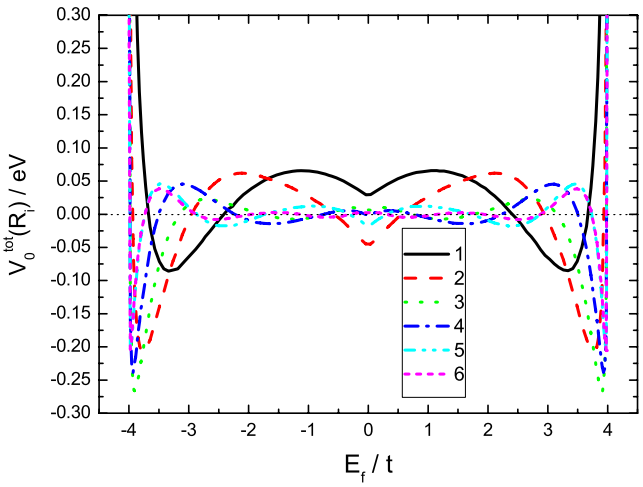

Figure 1. In the one-layer case, the screened potential energy (in units of eV) at the six nearest-neighbors surrounding the external point charge impurity at the origin as a function of Fermi energy $E_{\rm f}$ (in units of t). 1, 2, 3, 4, 5 and 6 correspond to lattice sites $(i_x, i_y) = (1, 0)$ (black solid), (1, 1) (red dashed), (2, 0) (green dotted), (2, 1) (blue dashed–dotted), (2, 2) (cyan dashed–double dotted) and (3, 0) (magenta short dashed), respectively.

As we can see, in the range of $E_{\rm f} = -3.65t$ to $E_{\rm f} = -2.42t$, the screened potential at the nearest-neighbor site $(1, 0)$ is attractive. As for the next-nearest-neighbor site $(1, 1)$, the screened potential energy is negative from $E_{\rm f} = -3.93t$ to $-2.96t$ and from $E_{\rm f} = -0.5t$ to 0. At about $E_{\rm f} = -3.91t$, the negative potential energy reaches a maximum magnitude at site $(2, 0)$, which is two lattice constants away from the impurity, and the potential energy is about -0.27 eV. The screened potential energy at other neighboring sites can also be negative, its magnitude is small in the range between $E_{\rm f} = -1.88t$ and 0. Close to $E_{\rm f} = -4t$, the magnitude becomes much larger, suggesting a strong attractive interaction between two like external charges. In the following, we will focus on the $E_{\rm f} = -3.91t$ and $-0.27t$ cases; they correspond to the maximum negative potential energy at all neighboring sites and the optimal doping level in cuprates, respectively. The number of electrons per site is $\langle n\rangle = 0.0145$ and 0.85 for the two cases, respectively.

In figure 2, we plot the screened potential energy as a function of the distance $|\boldsymbol{R}_i|$ between the origin and the lattice site (i_x, i_y), at $E_{\rm f} = -3.91t$ and $-0.27t$, respectively. In both cases, there is negative screened potential energy at certain neighboring sites of the impurity, leading to an attractive interaction between the external negative point charge at the origin and another negative charge at those neighboring sites. Here, we plot the results using both the Yukawa potential and Coulomb potential as the bare potential. As we can see, there are no qualitative differences between them, with only minor quantitative ones. So the Yukawa potential can well describe the long range characteristic of the system. If we increase the value of λ, finally the results will approach those (results) of the Hubbard model, which is beyond the scope of the current paper.

In order to investigate the impact of interlayer coupling on the dielectric screening, we first consider the two-layer case.

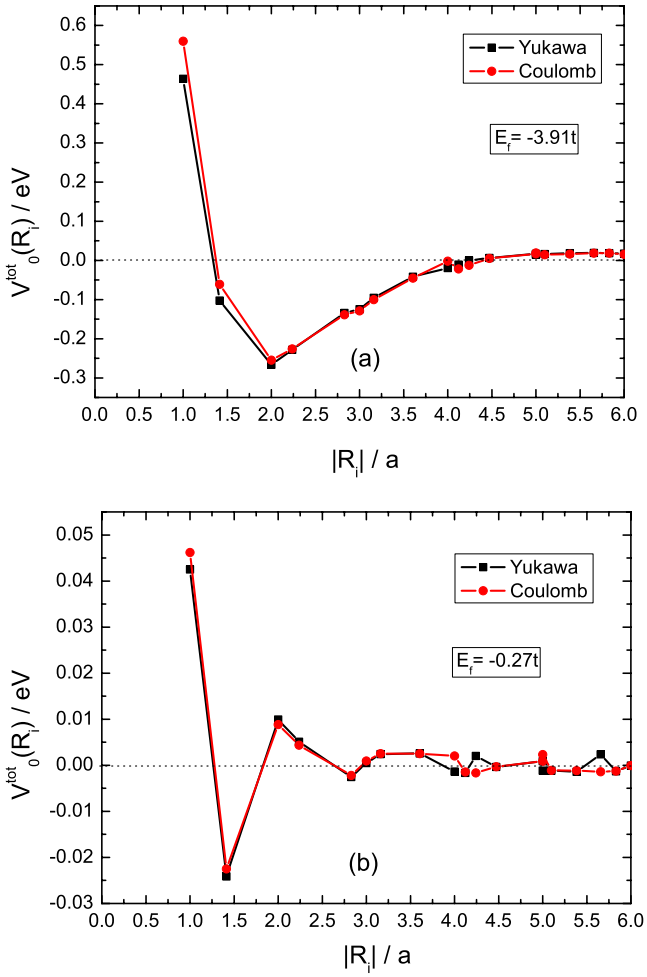

Figure 2. In the one-layer case, the screened potential energy (in units of eV) as a function of the distance $|\boldsymbol{R}_i|$ (in units of a) between the origin and the lattice site (i_x, i_y), at (a) $E_{\rm f} = -3.91t$ and (b) $E_{\rm f} = -0.27t$, using both Yukawa potential (black) and Coulomb potential (red) as the bare potential.

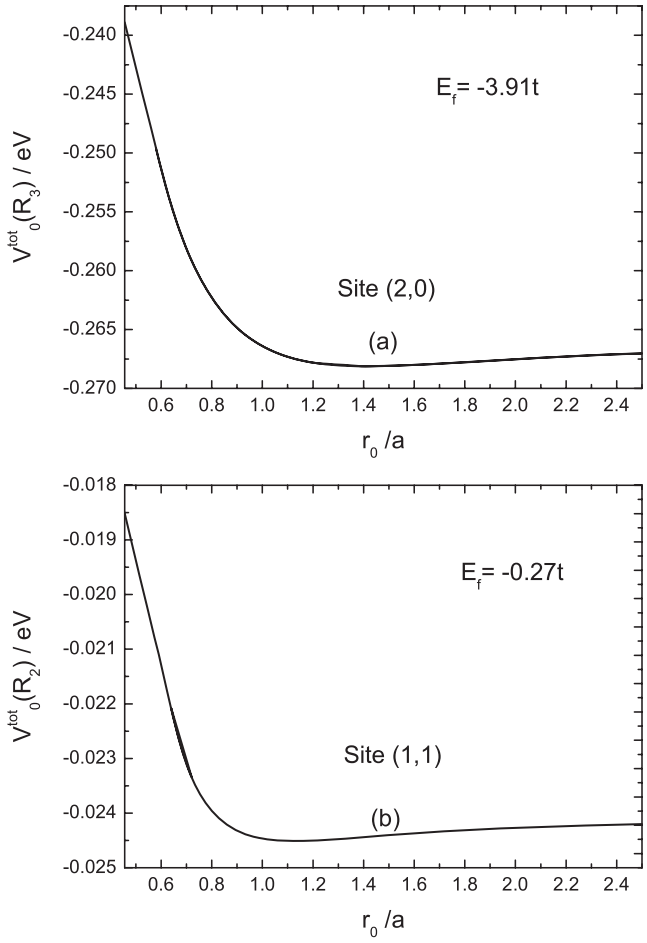

Figure 3. In the two-layer case, the screened potential energy (in units of eV) at the neighboring sites (in the $m = 0$ plane) of the external point charge impurity as a function of the interlayer distance r_0 (in units of a). (a) Site $(2, 0)$, $E_{\rm f} = -3.91t$ and (b) site $(1, 1)$, $E_{\rm f} = -0.27t$.

The impurity is located at the origin of the $m = 0$ plane and we add another ($m = 1$ layer) square lattice directly above the $m = 0$ plane. By solving (15), we have

$$V_{0q}^{\rm tot} = \frac{F_0(\boldsymbol{q}) + D(\boldsymbol{q})[F_1(\boldsymbol{q})^2 - F_0(\boldsymbol{q})^2]}{[1 - D(\boldsymbol{q})F_0(\boldsymbol{q})]^2 - [D(\boldsymbol{q})F_1(\boldsymbol{q})]^2},$$
$$V_{1q}^{\rm tot} = \frac{F_1(\boldsymbol{q})}{[1 - D(\boldsymbol{q})F_0(\boldsymbol{q})]^2 - [D(\boldsymbol{q})F_1(\boldsymbol{q})]^2}. \quad (22)$$

In the following, we will study mainly the screened potential energy at the neighboring sites (in the $m = 0$ plane) of the impurity and its relation to the interlayer distance r_0. Because of our choice of the on-site repulsive potential U, when the interlayer distance is smaller than $r_0^{\rm min}$, where $r_0^{\rm min}$ satisfies the relation $\exp(-\lambda r_0^{\rm min})/r_0^{\rm min} = U$, the bare interaction between the impurity and another negatively charged impurity at the site $(i_x, i_y) = (0, 0)$ in the $m = 1$ plane no longer obeys the Yukawa form. Instead, it is replaced by a constant U, regardless of r_0. So, we only consider what happens when $r_0 > r_0^{\rm min}$. Based on the parameters in our model, $r_0^{\rm min}$ is 0.456 (in units of a).

Since we are most interested in the neighboring site that has a larger magnitude of negative potential energy than other sites and from the results of the one-layer case shown in figure 2, we focus on the site $(i_x, i_y) = (2, 0)$ when $E_{\rm f} = -3.91t$ and site $(1, 1)$ when $E_{\rm f} = -0.27t$.

In figure 3, we plot the screened potential energy at the neighboring sites (in the $m = 0$ plane) of the impurity as a function of the interlayer distance r_0, at $E_{\rm f} = -3.91t$ and $-0.27t$, respectively. As we can see, the interlayer distance affects the screened potential energy in a similar way. When the interlayer distance is small, the addition of the $m = 1$ layer actually diminish the overscreening effect, compared to the one-layer case. The strength of the screened negative potential energy first increases with increasing interlayer distance, up to an optimal value $r_0^{\rm opt}$, where the negative potential energy reaches a maximum magnitude, which is larger than its one-layer counterpart, thus leading to an enhanced attractive interaction between the external negative point charge and another negative charge at that site. After that, the strength of the screened negative potential energy decreases with increasing interlayer distance, and finally converges to its one-layer value.

In figure 3(a), $E_f = -3.91t$, the screened potential energy at site $(2, 0)$ has a larger negative magnitude than other sites. At $r_0^{opt} = 1.41a$, corresponding to an interlayer distance 5.41 Å, the screened negative potential energy reaches a maximum magnitude, the strength of which is about 0.64% larger than that in the one-layer case.

Then when $E_f = -0.27t$, site $(1, 1)$ has the largest magnitude of screened negative potential energy. $r_0^{opt} = 1.14a$ (4.34 Å) and there is a 1.57% enhancement in this case, as shown in figure 3(b).

Next, we consider the three-layer case. Besides the $m = 0$ and 1 planes, we add a $m = -1$ plane, symmetric with the $m = 1$ plane (with respect to the $m = 0$ one). The external point charge impurity is still located at the origin. In this scenario, the screened potential energy in each of the planes is

$$\begin{aligned} V_{0q}^{tot} &= \{F_0(q) + D(q)[2F_1(q)^2 - F_0(q)^2 - F_0(q)F_2(q)]\} \\ &\quad \times \{[1 - D(q)F_0(q)]^2 - 2[D(q)F_1(q)]^2 - D(q)F_2(q) \\ &\quad + D(q)^2 F_0(q)F_2(q)\}^{-1}, \\ V_{1q}^{tot} &= \{F_1(q)\}\{[1 - D(q)F_0(q)]^2 - 2[D(q)F_1(q)]^2 \\ &\quad - D(q)F_2(q) + D(q)^2 F_0(q)F_2(q)\}^{-1}, \\ V_{-1q}^{tot} &= V_{1q}^{tot}. \end{aligned} \tag{23}$$

Then, we adopt a periodic condition along the e_z direction. Suppose there are $2N_\perp + 1$ layers with $m = -N_\perp, \ldots, 0, \ldots, N_\perp$ and the external point charge impurity is located at the origin. After Fourier-transforming V_{mq}^{tot} and $F_m(q)$ in the e_z direction, we get

$$V_{mq}^{tot} = \sum_{k_\perp=-N_\perp}^{N_\perp} V^{tot}(k_\perp, q) e^{i\frac{2\pi k_\perp m}{2N_\perp+1}}, \tag{24}$$

where

$$V^{tot}(k_\perp, q) = \frac{F(k_\perp, q)}{1 - (2N_\perp + 1)D(q)F(k_\perp, q)}, \tag{25}$$

and

$$F(k_\perp, q) = \frac{1}{2N_\perp + 1} \sum_{m=-N_\perp}^{N_\perp} F_m(q) e^{-i\frac{2\pi k_\perp m}{2N_\perp+1}}. \tag{26}$$

In our calculation, we take $N_\perp = 10$, so there are a total of 21 layers. In figure 4, we plot the comparison of the screened potential energy at the neighboring sites (in the $m = 0$ plane) of the impurity as a function of the interlayer distance r_0 in the two-layer, three-layer and periodic twenty-one-layer cases, at $E_f = -3.91t$ and $-0.27t$, respectively.

As we can see, the screened potential energy in the periodic twenty-one-layer case is barely distinguishable from the three-layer one, in the range of the interlayer distance considered in our calculation, suggesting the three-layer structure may be enough to account for the impact of interlayer coupling on the dielectric screening. So we can only compare the two-layer and three-layer cases. In both cases, the dependence of the screened potential energy on the interlayer distance shows some similarity, but there are still differences between them.

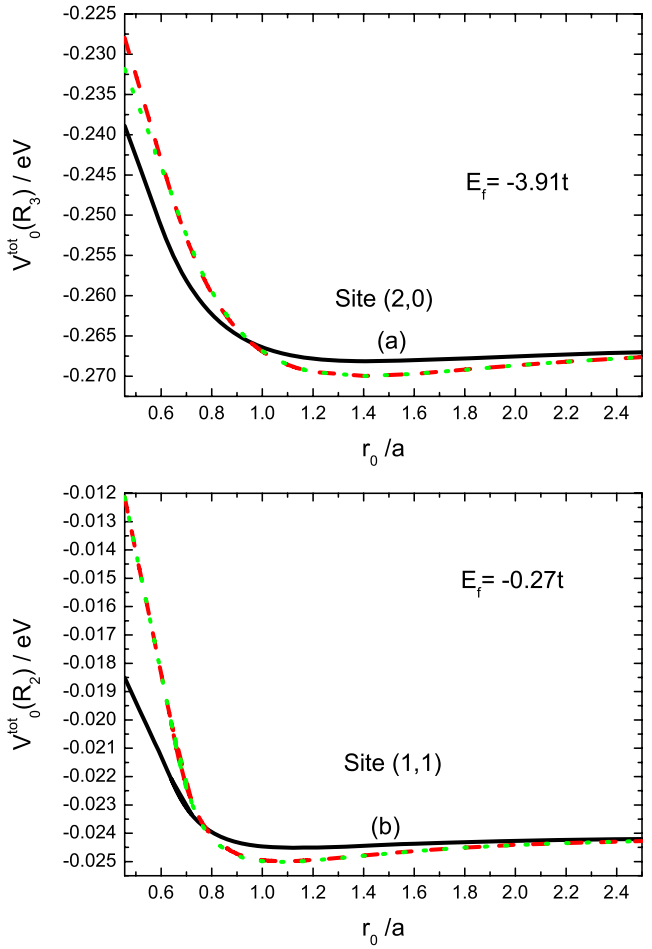

Figure 4. The comparison of the screened potential energy (in units of eV) at the neighboring sites (in the $m = 0$ plane) of the impurity as a function of the interlayer distance r_0 (in units of a) in the two-layer (black solid), three-layer (red dashed) and periodic twenty-one-layer (green dotted) cases. (a) Site $(2, 0)$, $E_f = -3.91t$ and (b) site $(1, 1)$, $E_f = -0.27t$.

In figure 4(a), $E_f = -3.91t$. When $r_0 < 0.96a$ (3.67 Å), two-layer has a stronger overscreening effect at site $(2, 0)$ than three-layer. After that, the trend reverses. In the three-layer case, the r_0^{opt} is also $1.41a$, coinciding with that in the two-layer one. The maximal strength of the negative potential energy increases by 1.33% with respect to the one-layer case, which doubles the enhancement of the two-layer case.

At $E_f = -0.27t$, compared to the two-layer case, the three-layer has a weaker overscreening effect at site $(1, 1)$ when $r_0 < 0.77a$ (2.96 Å) and a stronger one after that. The r_0^{opt} in the three-layer case is $1.09a$ (4.18 Å), which is slightly smaller than its two-layer counterpart. At this interlayer distance, the three-layer can enhance the magnitude of the screened negative potential energy by 3.56% with respect to the one-layer case, which is also about twice as large as the two-layer one, as can be seen in figure 4(b).

Finally, we investigate the impact of band structure on the screened potential. We add a next-nearest-neighbor hopping integral t' in (1). The dispersion now is

$$E(k) = -2t[\cos(k_x a) + \cos(k_y a)] - 4t' \cos(k_x a) \cos(k_y a). \tag{27}$$

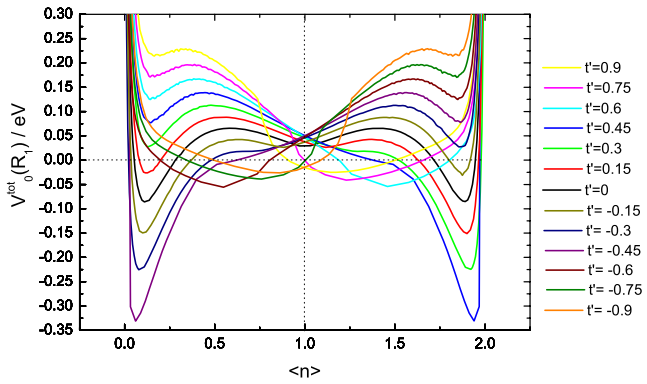

Figure 5. In the one-layer case, the screened potential energy (in units of eV) at the nearest-neighbor site (1, 0) of the external point charge impurity as a function of the number of electrons per site $\langle n\rangle$, at various value of the next-nearest-neighbor hopping integral t' (in units of t).

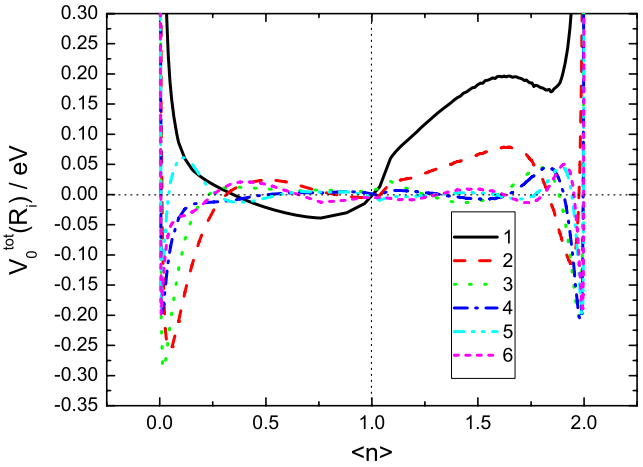

Figure 6. In the one-layer case, the screened potential energy (in units of eV) at the six nearest-neighbors surrounding the external point charge impurity at the origin as a function of the number of electrons per site $\langle n\rangle$, at $t' = -0.75$ (in units of t). 1, 2, 3, 4, 5 and 6 correspond to lattice sites $(i_x, i_y) = (1, 0)$ (black solid), (1, 1) (red dashed), (2, 0) (green dotted), (2, 1) (blue dashed–dotted), (2, 2) (cyan dashed–double dotted) and (3, 0) (magenta short dashed), respectively.

In figure 5, we plot the screened potential energy at the nearest-neighbor site (1, 0) of the external point charge impurity as a function of the number of electrons per site, $\langle n\rangle$, at various values of the next-nearest-neighbor hopping integral t' (in units of t) in the one-layer case. Due to the existence of the t' term, there is no particle and hole symmetry anymore, so the results are not symmetric with respect to $\langle n\rangle = 1$. But the results of t' and $-t'$ are symmetric with respect to $\langle n\rangle = 1$. This is because substituting $\boldsymbol{k}$ by $\boldsymbol{k}+(\pi/a, \pi/a)$ in (27) and changing t' to $-t'$ reverse the sign of $E(\boldsymbol{k})$. Because of this symmetry, we can focus on the $\langle n\rangle < 1$ side. As we can see, from $t' = 0.75$ to 0.3, there is no overscreening, but the $t' = 0.9$ case is an exception; there exists overscreening from $\langle n\rangle = 0.92$ to $\langle n\rangle = 1$. From $t' = 0.15$ to -0.9, there are overscreening regions on the $\langle n\rangle < 1$ side, but there are differences among them: from $t' = 0.15$ to -0.45, the maximum magnitude of the negative potential energy is increasing with decreasing t' and it appears at almost the same $\langle n\rangle$, at about $\langle n\rangle = 0.1$. Also, the overscreening region is enlarging with decreasing t'. From $t' = -0.6$ to -0.9, the overscreening region is shifted towards half-filling. At $t' = -0.75$, we plot the screened potential energy at the neighboring sites of the external point charge impurity as a function of the number of electrons per site $\langle n\rangle$ in figure 6. It is remarkable that the potential near half-filling on the $\langle n\rangle < 1$ side resembles the effective potential postulated in the tUV model [35]. This is a situation where one has a dominant nearest-neighbor attractive pair potential near half-filling, which is favorable for the cuprates to produce d-wave pairing. A realistic value of t' in the cuprates is about -0.45 [36], which is not quite as negative as we would like it to be, but it is not too far away either; at least the sign is right.

4. Conclusions

In conclusion, we have studied the dielectric screening of an external point charge in a layered lattice electron gas by using the random phase approximation. The effective interaction between two neighboring point charges (of the same sign) is found to be attractive over a wide range of interlayer distances. The effect of different numbers of layers on this interaction is studied. We have also investigated the impact of band structure on this screened potential. It seems that overscreening can depend significantly on detailed band structures as noted by Lin and Shung [31] before. The addition of an diagonal hopping term (t') is essential in obtaining nearest-neighbor overscreening near half-filling.

We note that, although part of our results resembles the continuum model calculation of Visscher and Falicov [28], there are important differences. Our results apply in the high density regime where the random phase approximation is better justified. The interesting band effects, such as the significant variations of potentials with band filling and the discrete separation between the impurities, are of course absent in the earlier treatments. Compared to the work done by Choy and Das [37], where they derived an attractive pairing potential from a repulsive Hubbard model in some region of the momentum space, we obtain a nearest-neighbor attractive potential in the real space, which is essential in explaining the phenomenology of cuprates.

Finally, it would be of further interest to go beyond the random phase approximation [29, 38] to calculate more accurately the pair potential. Although the effective electron–electron interaction is, in general, more complicated than the pair potential between two external point charges, our results provide a possible source of the intersite attractive interaction in the extended Hubbard model. In addition, our results could be relevant to the behavior of a collection of charged species such as impurities or dopants near the conduction planes. The attraction may lead to phase separation of the species.

Acknowledgments

We thank Dr C S Ting for helpful discussions. This work was supported by the Texas Center for Superconductivity and the Robert A Welch Foundation (grant no. E-1070).

References

[1] Bednorz J G and Müller K A 1986 *Z. Phys.* B **64** 189
[2] Wu M K *et al* 1987 *Phys. Rev. Lett.* **58** 908
[3] Kamihara Y *et al* 2006 *J. Am. Chem. Soc.* **128** 10012
[4] Kamihara Y *et al* 2008 *J. Am. Chem. Soc.* **130** 3296
[5] Ren Z-A *et al* 2008 *Mater. Res. Innovat.* **12** 105
[6] Chen G F *et al* 2008 *Phys. Rev. Lett.* **101** 057007
[7] Chen X H *et al* 2008 *Nature* **453** 761
[8] Chen G F *et al* 2008 *Phys. Rev. Lett.* **100** 247002
[9] McCann E and Falko V I 2006 *Phys. Rev. Lett.* **96** 086805
[10] Nilsson J *et al* 2006 *Phys. Rev.* B **73** 214418
[11] Partoens B and Peeters F M 2006 *Phys. Rev.* B **74** 075404
[12] Koshino M and Ando T 2006 *Phys. Rev.* B **73** 245403
[13] Snyman I and Beenakker C W J 2007 *Phys. Rev.* B **75** 045322
[14] Morozov S *et al* 2008 *Phys. Rev. Lett.* **100** 016602
[15] Novoselov K *et al* 2006 *Nat. Phys.* **2** 177
[16] Oostinga J *et al* 2008 *Nat. Mater.* **7** 151
[17] Hwang E H and Das Sarma S 2008 *Phys. Rev. Lett.* **101** 156802
[18] Micnas R, Ranninger J, Robaszkiewicz S and Tabor S 1988 *Phys. Rev.* B **37** 9410
[19] Martin I *et al* 2001 *Europhys. Lett.* **56** 849
[20] Micnas R *et al* 1990 *Rev. Mod. Phys.* **62** 113
[21] Bari R A 1971 *Phys. Rev.* B **3** 2662
[22] Anderson P W 1975 *Phys. Rev. Lett.* **34** 953
[23] Alexandrov A and Ranninger J 1981 *Phys. Rev.* B **23** 1796
[24] Hirsch J E and Scalapino D J 1985 *Phys. Rev.* B **32** 117
[25] Robaszkiewicz S, Micnas R and Chao K A 1981 *Phys. Rev.* B **23** 1447
[26] Alexandrov A S, Ranninger J and Robaszkiewicz S 1986 *Phys. Rev.* B **33** 4526
[27] Robaszkiewicz S, Micnas R and Ranninger J 1987 *Phys. Rev.* B **36** 180
[28] Visscher P B and Falicov L M 1971 *Phys. Rev.* B **3** 2541
[29] Malozovsky Y M and Fan J D 1994 *Phys. Rev.* B **49** 4334
[30] Hawrylak P 1987 *Phys. Rev. Lett.* **59** 485
[31] Lin M F and Shung Kenneth W-K 1992 *Phys. Rev.* B **46** 12656
[32] Raghu S *et al* 2008 *Phys. Rev.* B **77** 220503(R)
[33] Seo K, Bernevig B A and Hu J P 2008 *Phys. Rev. Lett.* **101** 206404
[34] Ehrenreich H and Cohen M H 1959 *Phys. Rev.* **115** 786
[35] Su W P 2005 *Mod. Phys. Lett.* B **19** 1295
[36] Leggett A J 1994 *Physica* B **199** 291
[37] Choy T C and Das M P 1993 *Phys. Rev.* B **47** 8942
[38] Yan X Z and Ting C S 2007 *Phys. Rev.* B **75** 035342